Available online at www.sciencedirect.com
ScienceDirect
Trans. Nonferrous Met. Soc. China 26(2016) 2523−2531
Transactions of Nonferrous Metals Society of China
www.tnmsc.cn

Grain boundary pre-precipitation and its contribution to enhancement of corrosion resistance of Al−Zn−Mg alloy

Hui-zhong LI[1,2,3], San-cheng YAO[1], Xiao-peng LIANG[1,2,3], Yong-hui CHEN[1], Chao LIU[1], Lan HUANG[3]

1. School of Materials Science and Engineering, Central South University, Changsha 410083, China;
2. Key Laboratory of Nonferrous Metal Materials Science and Engineering, Ministry of Education, Central South University, Changsha 410083, China;
3. State Key Laboratory of Powder Metallurgy, Central South University, Changsha 410083, China

Received 11 October 2015; accepted 8 April 2016

Abstract: High temperature pre-precipitation (HTPP) took place in 7005 alloy at various temperatures after solution treatment and its influence on mechanical properties, corrosion behaviors and microstructure of the alloy was investigated using tensile test, intergranular corrosion (IGC) test, slow strain rate testing (SSRT), together with microstructural examinations. It is found that Vickers hardness of the aged alloy decreases gradually with decreasing the HTPP temperature, and almost a reverse trend of electrical conductivity is found compared to the hardness changes. Depending on the changes, two HTPP temperatures of 440 and 420 °C were chosen for comparative study. Results reveal that HTPP alloy tempers exhibit higher resistance to stress corrosion cracking (SCC) and IGC than none pre-precipitate one with an acceptable strength loss due to the substantial enhancement of distribution discontinuity of the coarse grain boundary precipitates (GBPs), and the coarsening and interspacing effect on GBPs becomes more obvious with decreasing the pre-precipitation temperature.

Key words: 7005 aluminum alloy; grain boundary pre-precipitation; stress corrosion cracking; intergranular corrosion; microstructure

1 Introduction

The heat treatable 7xxx series aluminum alloys have been extensively developed and used as advanced structural materials in military aircraft as well as commercial transportation industry due to a good combination of low density, high specific strength, satisfactory ductility and resistance to fatigue [1]. These alloys, unfortunately, are very vulnerable to stress corrosion cracking (SCC) in aqueous salt solution containing particularly the chlorine ions [2,3]. Besides, other forms of localized corrosion also occur under humid atmosphere and industrial waste gas, such as intergranular corrosion (IGC).

Up to the present, efforts have been made through heat treatments to overcome or reduce the SCC susceptibility of high strength 7xxx series aluminum alloys. It has been found that over-aged (T7x aging, with a strength loss of 10%−15% compared with that of T6 temper) or complicated retrogression and re-aged (RRA, without loss of strength) treatment can notably reduce the susceptibility of these alloys to SCC [2,3−5]. Nevertheless, correlations between grain boundary microstructures and SCC susceptibility for the over-aged alloys have not been fully established. The proposed mechanisms [6−8] to explain the beneficial effects of over-aging on SCC resistance are still controversial and none of these mechanisms can explain all the SCC experimental results. RRA treatment, an aging schedule which can optimize both strength and SCC resistance of these alloys, is inappropriate for large-section components owing to the request for a short retrogression time. Apart from aging, solution and quenching treatment is another important factor that has great effect on microstructure, and thus on localized corrosion behaviors. LIN et al [9] and OU et al [10] indicated that step-quenching and aging can modify the SCC resistance of 7050 alloy. CHEN et al [11] studied the effect of quenching rate on microstructure and SCC

Foundation item: Project (51301209) supported by the National Natural Science Foundation of China
Corresponding author: Xiao-peng LIANG; Tel: +86-731-88830377; Fax: +86-731-88830257; E-mail: liangxp@csu.edu.cn
DOI: 10.1016/S1003-6326(16)64378-9

of 7085 alloy, and it was found that the improved SCC resistance is attributed to the relative high Cu content and large interspace of grain boundary precipitates (GBPs). HUANG et al [12,13] reported that high temperature pre-precipitation (HTPP) treatment not only keeps the high strength of 7A52 and 7055 alloy, but also enhances the resistance to IGC and SCC. In general, previous works showed that microstructure and microchemistry about localized corrosions including GBPs, matrix nearby and precipitate free zones (PFZ) can be controlled by heat treatments to improve the corrosion resistance [14−16].

7005 aluminum alloy has a long history, and it is still widely used in rail transit industry. However, little information is available in references about the effect of HTPP treatment on mechanical properties, localized corrosions and microstructure in mid-strength aluminum alloy. In this work, an attempt has been made to study the effect of HTPP treatment on mechanical properties, localized corrosion behaviors and microstructure of a mid-strength 7005 aluminum alloy, and the localized corrosion process and mechanism were also briefly analyzed.

2 Experimental

Hot extruded 7005 alloy plate with a thickness of 8.0 mm was used for this study. Nominal chemical composition of which is shown as follows: 4.15 Zn, 1.27 Mg, 0.017 Cu, 0.15 Fe, 0.14 Si, 0.29 Mn, 0.20 Cr, 0.10 Zr, 0.035 Ti, 0.01 V (mass fraction, %) and balance Al. A two-staged solution treatment was carried out, i.e., all the specimens were held at 450 °C for 30 min and ramped up to 470 °C for 30 min again and then ramped down to a temperature of 460, 440, 420, 400, 380, 370 and 360 °C respectively for another 30 min before quenching in water at room temperature followed by T6 artificial aging at 120 °C for 42 h. During the pre-precipitation process, temperature dropped at a controlled cooling rate of 1 °C/min from 470 °C to 460, 440, 420, 400, 380, 370 and 360 °C, respectively. Specimen hardness and conductivity measurements were used to monitor value changes during pre-precipitation process and the values reported here represented an average of at least 5 individual measurements. Accelerated IGC tests were performed according to the test standard of GB/T 7998—2005 [17], and the maximum depth of attack was measured and defined as the IGC susceptibility.

Slow strain rate tests (SSRT) were carried out at an initial strain rate of 1.0×10^{-6} s^{-1} in dry air and in aqueous 3.5% NaCl solution (mass fraction) on a slow strain rate tensile machine (LETRY WDML−1) at room temperature. The gauge portion of the SSRT specimen, made from the longitudinal direction of the alloy plate, having dimensions of 25 mm × 5 mm with a thickness of 3.0 mm was metallographically abraded and polished to produce scratch-free smooth surface. Failed specimen surfaces after SSRT were observed using a scanning electron microscopy (Sirion200) operated at 15 kV.

The relative ductility loss, $I_{SCC}(\delta)$, is defined as the SCC susceptibility [18],

$$I_{scc}(\delta)=\left(1-\frac{\delta_{sol.}}{\delta_{air}}\right)\times100\% \quad (1)$$

where $\delta_{sol.}$ and δ_{air} are the elongations of the specimens in test solution and in dry air, respectively.

All samples for TEM observations were taken from sections perpendicular to the extruding direction and electropolished in a solution of 30% HNO_3 in CH_3OH at about −25 °C and 16 V. The thin foils were examined by a transmission electron microscope (Tecnai G^2 20ST) operated at 200 kV.

Electrochemical measurement was carried out using a three-electrode cell, furnished with a saturated calomel reference electrode (SCE) and a platinum sheet counter electrode. The studied alloy with an exposed square surface of 1 cm^2 acted as the working electrode. Potentiodynamic polarization tests were carried out at the applied potential, ranging from −0.2 to 0.2 V (vs OCP) in aqueous 3.5% NaCl solution with a scan rate of 1.0 mV/s. Cview program was used for data fitting of polarization curves.

The polarization resistance, R_p, was calculated according to the following equation [19]:

$$\frac{1}{R_p}=2.303J_{corr}\left(\frac{1}{b_a}+\frac{1}{|b_c|}\right) \quad (2)$$

where b_a, b_c and J_{corr} refer to the anodic Tafel slope, cathodic Tafel slope and corrosion current density, respectively.

3 Results

3.1 Hardness, conductivity and tensile properties

The initial as-extruded alloy was subjected to a two-staged solution treatment, i.e., held at 450 °C and 470 °C for 30 min respectively and then ramped down to a temperature of 460, 440, 420, 400, 380, 370 and 360 °C respectively for another 30 min before quenching in water at room temperature followed by an artificial aging at 120 °C for 42 h. Effect of various HTPP temperatures on Vickers hardness and conductivity of the aged specimen is shown in Fig. 1. Generally, the aged specimen hardness decreases gradually with the decrease of HTPP temperature. No obvious changes were monitored in hardness of the aged specimen after solution (pre-precipitation) treatment when the pre-precipitation temperature is close to the solution treatment temperature. Besides, the hardness value of the specimen pre-precipitated at 460 °C is basically similar to that of the specimen heat treated at 470 °C without the pre-precipitation treatment. A further decrease in hardness takes place with the further decrease of pre-precipitation temperature. Note that almost a reverse trend of electrical conductivity is found compared to the hardness changes.

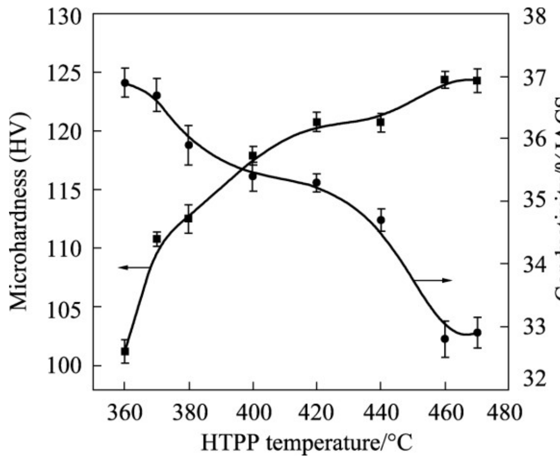

Fig. 1 Variations of hardness and conductivity with HTPP temperatures of aged alloy specimen after two-staged solution treatment

Based on the hardness and conductivity changes, two pre-precipitation temperatures of 440 °C and 420 °C were chosen for SCC susceptibility evaluations and microstructure observations. The tensile properties of the investigated alloys denoted as NP, 440P and 420P (Table 1) are listed in Table 2. It shows that NP alloy has the highest tensile strength, while the yield strengths (YS) and ultimate tensile strengths (UTS) of 440P and 420P alloys decrease by ~5%. Moreover, the YS and UTS of 420P alloy are basically similar to those of 440 P alloy.

Table 1 Solution (pre-precipitation) and aging process parameters of studied alloy

Sample No.	Solution (pre-precipitation)	Aging
NP	(450 °C, 30 min) + (470 °C, 30 min)	120 °C, 42 h
440P	(450 °C, 30 min) + (470 °C, 30 min) + (440 °C, 30 min)	
420P	(450 °C, 30 min) + (470 °C, 30 min) + (420 °C, 30 min)	

3.2 IGC behavior

The microstructural characterizations of cross section for the alloy samples exposed to IGC test solution for 6 h are presented in Fig. 2. The corrosion cracks initiated from the outside, propagating to the inside under the surface along the long-transverse direction of the alloy matrix. Evident network-shaped IGC occurred in NP alloy, and the maximum attack depth of NP alloy is 53.6 μm, whereas those on 440P and 420P alloy samples are 26.5 and 19.8 μm, respectively. The obvious difference on the maximum attack depth indicates that HTPP treatment can decrease the susceptibility to IGC.

3.3 SCC susceptibility

Typical nominal stress and nominal strain curves of three temper alloys tested in dry air and in naturally aerated 3.5% NaCl solution are exhibited in Fig. 3. It is apparent that the SCC susceptibility of NP, 440P and 420P alloys are significantly different. According to Eq. (1), the $I_{SCC}(\delta)$ of three temper alloys are calculated and summarized in Table 2. A high $I_{SCC}(\delta)$ value suggests high SCC susceptibility. NP alloy has the greatest ductility loss and SCC susceptibility, and variation of the tensile strengths of specimens tested in air and in 3.5% NaCl solution is the greatest. It means that not only the ductility but also tensile strength of NP alloy is damaged in 3.5% NaCl solution. While 420P alloy has the lowest ductility loss and SCC susceptibility compared to NP alloy, and 420P alloy scarcely has the strength damaged. The calculations for relative ductility loss of various alloy tempers demonstrate that the SCC resistance of the peak-aged alloy could be improved via the HTPP treatment, and the resistance to SCC can enhance by decreasing the HTPP temperature.

3.4 SEM fractographs and longitudinal section observations after SSRT

The fracture surfaces of SSRT specimens failed in dry air appear the similar features, composing of equiaxial dimples of various sizes consistently, as shown in Figs. 4(a)−(c). Figure 4(d), the fractograph of failed NP alloy specimen tested in 3.5% NaCl solution, exhibits prominent cleavage crack feature, presence of a few intergranular cracks, secondary cracks and very fine shallow flat dimples in some of the grains as well. Rock

Table 2 Mechanical properties and SCC susceptibilities for studied alloy

Sample No.	Ultimate tensile strength/MPa	Yield strength/MPa	Tensile elongation/%	Elongation loss after SSRT/%	Deepest crack length after SSRT/μm
NP	376.8	291.9	13.2	25.75	55.31
440P	355.1	273.8	16.4	13.81	25.38
420P	356.6	278.5	13.6	8.41	16.13

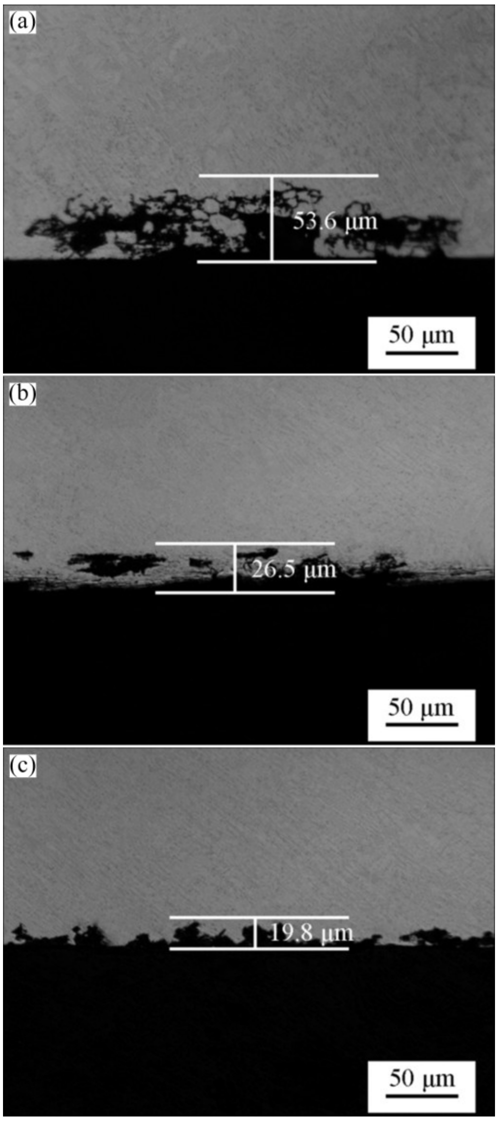

Fig. 2 Micrographs of cross section (perpendicular to extruded direction) for investigated alloy exposed to IGC environment for 6 h: (a) NP; (b) 440P; (c) 420P

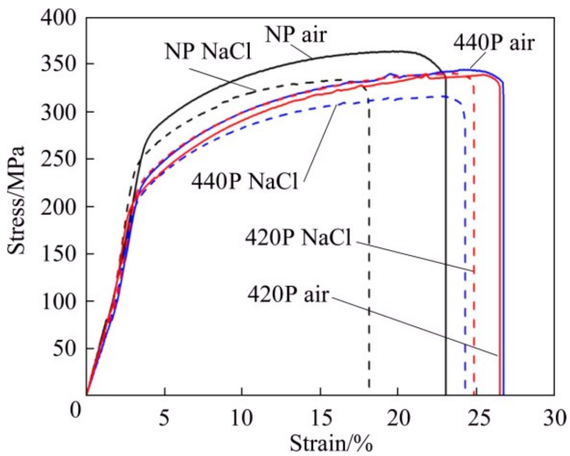

Fig. 3 Typical SSRT curves of three temper alloys tested in dry air and in naturally aerated 3.5% NaCl solution with initial strain rate of 1.0×10^{-6} s^{-1} at room temperature

candy structure on the overall fracture surface is observed, which means a typical brittle fracture appearance. However, the fractograph of 440P alloy (Fig. 4(e)) displays a mixed mode fracture nature. There are no signs of intergranular cracking or obvious cleavage facets, but larger and deeper dimples of various sizes are visible. Furthermore, as illustrated in Fig. 4(f), a typical ductile transgranular fracture feature can be clearly seen in 420P alloy specimen, predominantly large and deep dimples, which indicates that a certain amount of deformation was still in it. In general, equiaxial dimples become more and deeper by the decrease of the HTPP temperature.

Metallographs of the longitudinal sections of the specimens after SSRT in 3.5% NaCl solution are presented in Fig. 5. A few of pits, acted as stress raiser and cracks as well, have been originated from the base of these pits and propagated, as revealed in Fig. 5(a). Further, it can be clearly seen that intergranular cracks initiated from the surface, propagating along the grain boundaries in NP alloy, while no apparent intergranular cracking characteristic is found for 440P alloy and 420P alloy as illustrated in Figs. 5(b) and (c). Statistical measurements of the deepest crack lengths of the longitudinal sections were conducted and the results are listed in Table 2. The deepest crack lengths of varied alloy tempers are 55.31, 25.38 and 16.13 μm for NP, 440P and 420P alloys, respectively, which further indicates that NP alloy has the highest SCC susceptibility, while 420P alloy has the lowest. The SCC susceptibilities of various tempers evaluated by the deepest crack length on the longitudinal sections of the specimens after SSRT in 3.5% NaCl solution are in good agreement with the obtained SSRT results and the fractographs of the tensile specimens.

3.5 Microstructure

Figure 6 shows the bright field TEM images of various alloys. Figures 6(a) and (b) illustrate the TEM images of the as-quenched alloy annealed at 470 °C for 30 min. No clearly discernable particles other than the spherical Al_3Zr dispersoids [20] could be observed. Dislocation loops generated during the quenching treatment which are considered to be a responsible factor for the SCC [21,22]. Figures 6(c) and (d) show the TEM images of grain boundary microstructure of the as-quenched alloys pre-precipitated at 440 °C and 420 °C for 30 min, respectively. Coarse and discrete rod-shaped GBPs ($MgZn_2$) are revealed, and the GBPs of 420P alloy are coarser and sparser than that of 440P alloy. Further, no detectable matrix precipitates (MPTs) appear in both two pre-precipitated tempers. Figures 6(e)−(g) show the TEM images of the aged alloy. Great amounts of fine metastable η' phases are distributed homogeneously

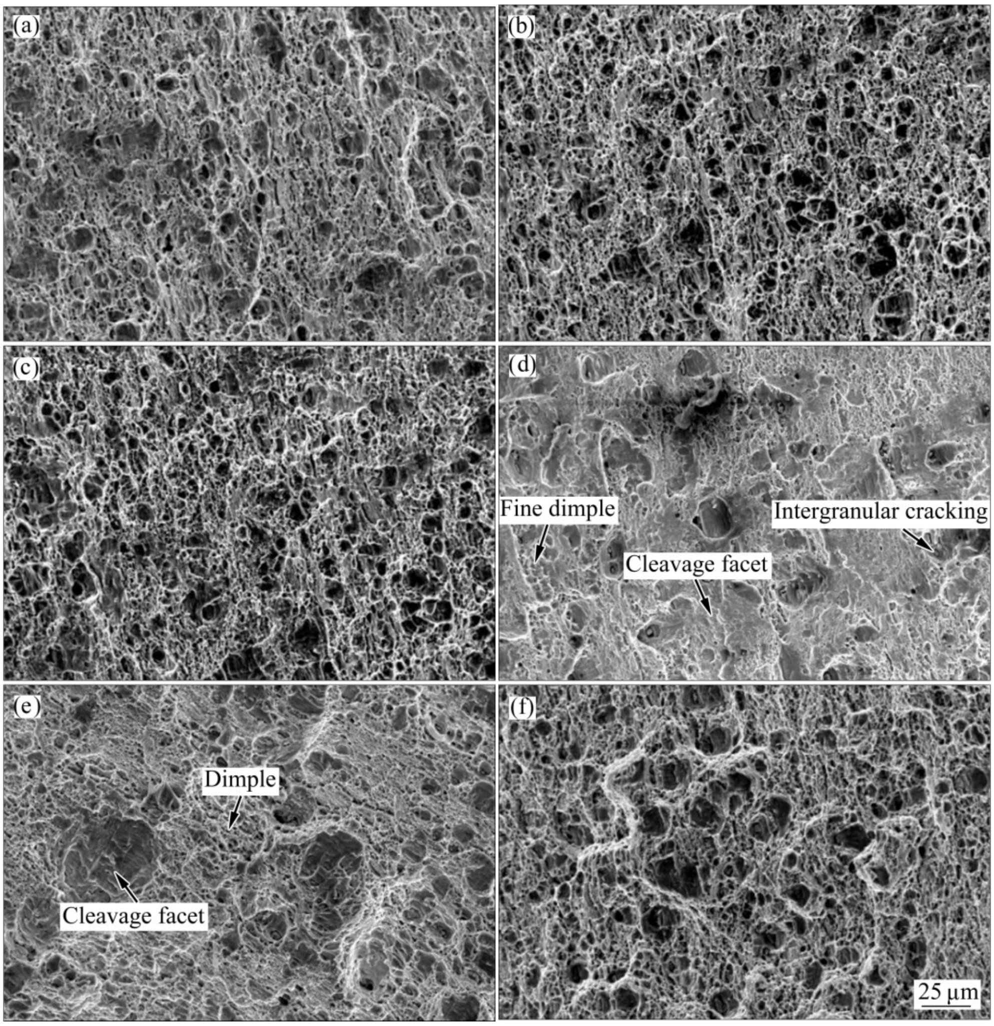

Fig. 4 SEM fractographs of SSRT specimens tested in dry air (a, b, c) and in naturally aerated 3.5% NaCl solution (d, e, f) at room temperature: (a, d) NP; (b, e) 440P; (c, f) 420P

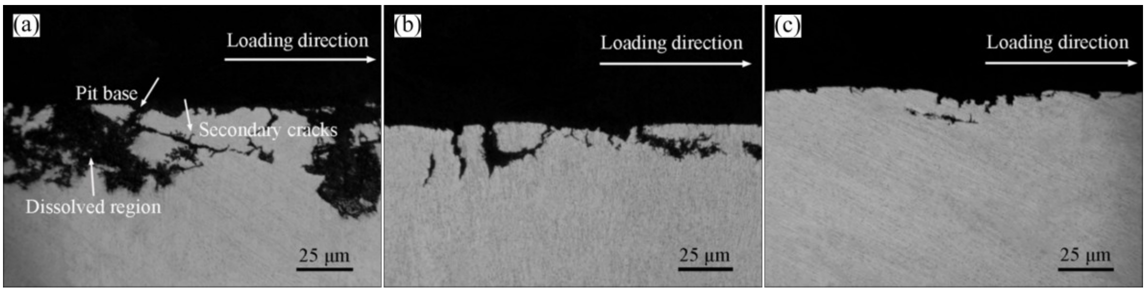

Fig. 5 Metallographs of longitudinal sections of specimens after SSRT in 3.5% NaCl solution at room temperature: (a) NP; (b) 440P; (c) 420P

within the matrix of the NP alloy, and the GBPs are small in size and distributed continuously along the grain boundary, as shown in Fig. 6(e). The preferentially precipitated equilibrium η phases after the HTPP treatment at 440 °C and 420 °C grew, aggregated, coarsened and accelerated the grain boundary precipitation during the subsequent aging process, which contributes to the formation of distinctly coarsened and widely spaced GBPs as shown in Figs. 6(f) and (g). In addition, the lower the HTPP pre-precipitation temperature, the more obvious this coarsening and interspacing effect on two adjacent GBPs. Figure 6(h) corresponds to $[011]_{Al}$ diffraction pattern (DP) of the aged 420P alloy. The main strengthening precipitates of the aged 420P alloy are still the η' phases.

3.6 Polarization test

The polarization plots of various alloy tempers in

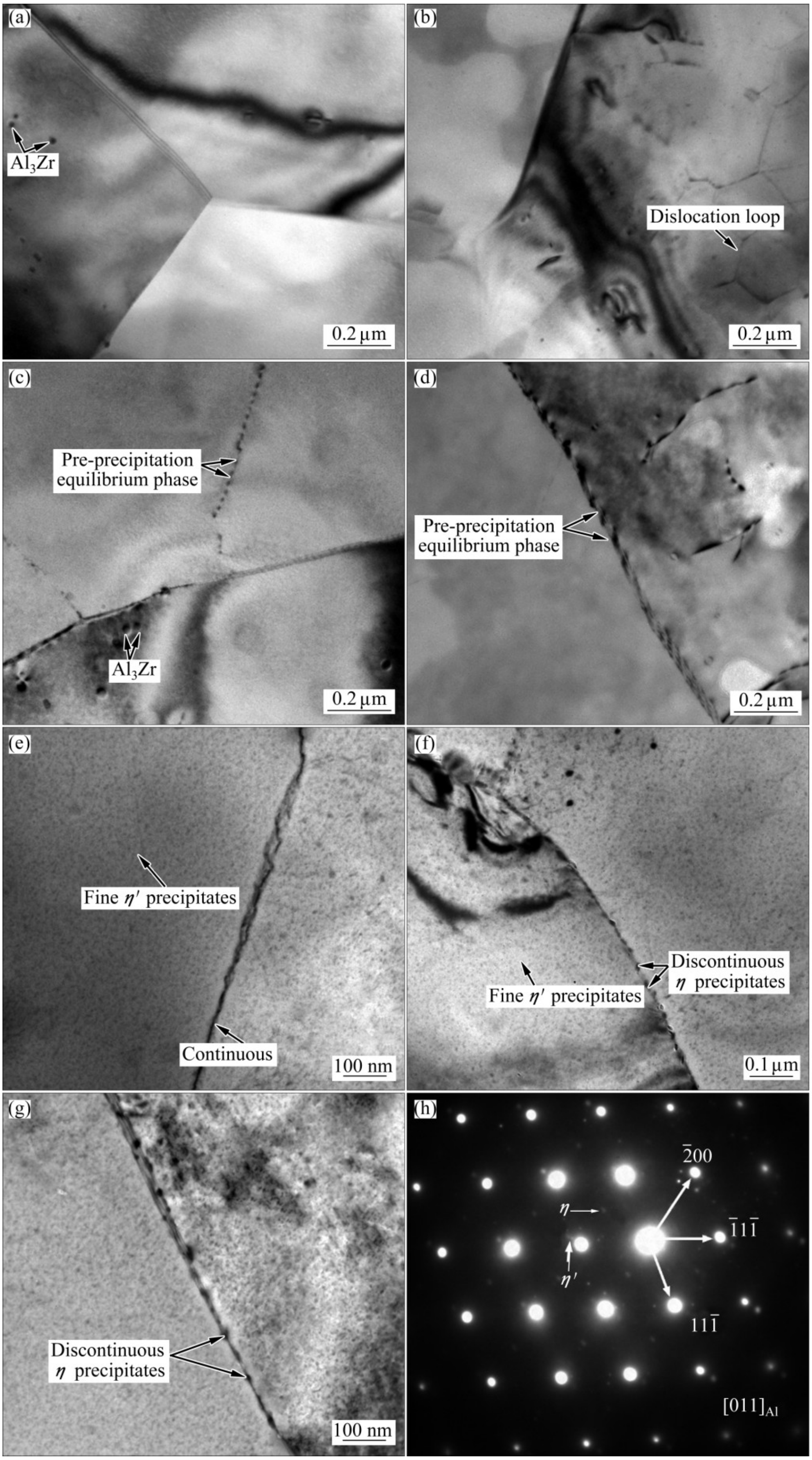

Fig. 6 Bright field TEM images of as-quenched and aged alloy: (a, b) As-quenched NP; (c) As-quenched 440P; (d) As-quenched 420P; (e) As-aged NP; (f) As-aged 440P; (g) As-aged 420P; (h) $[011]_{Al}$ DP corresponding to fine precipitates in (g)

Table 3 Electrochemical characteristics of various alloy tempers in naturally aerated 3.5% NaCl solution derived from polarization plots

Sample No.	Corrosion potential, φ_{corr}(vs SCE)/V	Current density, J_{corr}/(A·cm^{-2})	Cathodic slope, b_c/(mV·decade^{-1})	Anodic slope, b_a/(mV·decade^{-1})	Polarization resistance, R_p/(Ω·cm^2)
NP	−0.873	2.2696×10^{-5}	−444.3	24.3	44.08
440P	−0.907	4.5182×10^{-6}	−705.7	25.4	235.62
420P	−0.902	3.9738×10^{-6}	−346.9	24.0	245.28

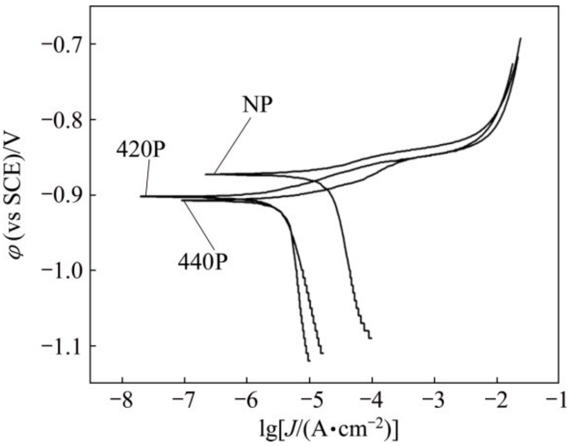

Fig. 7 Typical potentiodynamic polarization plots for various alloy tempers in naturally aerated 3.5% NaCl solution

3.5% NaCl solution and corresponding corrosion parameters derived from these plots using Tafel analysis are presented in Fig. 7 and Table 3, respectively. The anodic sides of the three curves exhibit a similar characteristic, which is controlled by anodic dissolution reaction. The values of φ_{corr} of the three tempers are close to each other. However, corrosion current density of 420P alloy decreases by 80.1% with respect to that of NP alloy. From another point of view [23], the electrochemical corrosion rate increases linearly with the corrosion current density by Faraday's law. Thus, from the electrochemical results, it can be inferred that 420P alloy has the highest corrosion resistance, namely the lowest corrosion susceptibility compared to other two alloy tempers, which is consistent with the observed IGC, SSRT results and the TEM microstructural features.

4 Discussion

4.1 Effect of HTPP treatment on corrosion

From the results of IGC, SSRT and complementary polarization tests, it can be concluded that HTPP treatment enhances the resistance to localized corrosions of the studied 7005 alloy, and the corrosion resistance increases with the decrease of temperature during the HTPP treatment. This is similar to the results in some previous investigations on other alloys such as 7055 and 7075 alloy [2,12]. Predominantly localized corrosions occur and develop along the grain boundaries (Fig. 2(a) and Fig. 5(a)), so it is reasonable to believe that the enhanced resistance to localized corrosions due to HTPP treatment was primarily caused by the changes in microstructure and microchemistry near the grain boundaries.

It is generally accepted that the main precipitates at grain boundaries of 7xxx series Al alloys are η ($MgZn_2$) phases. In Refs. [24,25], it was reported that the φ_{corr} of PFZ, equilibrium η phase at the grain boundary and aged alloy matrix are −0.57, −0.86 and −0.68 V, respectively. The potential of η phase is more negative than that of the matrix nearby, consequently, η phase is anodic to attack and dissolved preferentially in corrosive environment. After initiation, corrosion develops along the anodic path of grain boundaries into the bulk alloy. It has been suggested that the continuous networks of η phases at the grain boundaries can promote self-dissolution and propagation in Al alloys and give rise to SCC and IGC failures. As shown in Fig. 6, the precipitates along grain boundaries of NP alloy distribute continuously and appear as chain-like, thus the grain boundaries are more inclined to become the corrosion channel for SCC and IGC. 440P alloy shows the distribution discontinuity in the presence of GBPs relatively, the anodic corrosion channel is cut off, hence the corrosion rate is decreased to some extent. The distribution discontinuity of GBPs increases with the decrease of HTPP temperature. Furthermore, the size of GBPs increases simultaneously with the decrease of HTPP temperature. Larger and sparser GBPs can inhibit corrosion propagation along the grain boundaries and reduce H concentration by acting as trapping sites to eliminate the negative effect of H atom on metal atom-bonding [10]. From Refs. [2,12], the Cu content of GBPs is related to the HTPP temperature. The lower the pre-precipitation temperature is, the higher the Cu content of GBPs is. For the 420P alloy temper, the lowest SCC susceptibility is attributed to not only the increase of size and interspace for GBPs, but also the increase of Cu content in GBPs. The increased Cu content in GBPs decreases the potential difference between matrix and GBPs, and delays the corrosion cracking initiation. The mechanism of SCC has been received intensive investigations, and it is proposed that either the anodic dissolution of Mg-rich phases or hydrogen embrittlement operated in the SCC process [6,24]. The anodic dissolution theory is always associated with intergranular fracture [6,14]. Seen from Fig. 4, NP alloy represents typical intergranular fracture, while 440P and 420P alloys represent typical ductile transgranular fractures, which indicates that anodic dissolution should be the main SCC mechanism for NP alloy, and hydrogen induced cracking for another two alloys.

4.2 Effect of HTPP treatment on age hardening

The supersaturated solution degree of the quenched alloy matrix decreases gradually with the decrease of HTPP temperature due to a small quantity of equilibrium precipitates formed in the grain boundaries and even the grain interiors as well, leading to less efficient age hardening. As shown in Fig. 1, when the alloy was subjected to pre-precipitation for 30 min at 460 °C, no hardness change was monitored for the reason that it was very close to the solution temperature, and the driving force of precipitation was small. When the alloy was pre-precipitated at a lower temperature (under 400 °C), the driving force of precipitation would increase to a certain extent, resulting in a considerable number of coarse and incoherent-type precipitates formed in the grain boundaries and even the grain interiors as well. On the other hand, the lower HTPP temperature is, the greater the loss of vacancies in matrix is, also leading to less efficient age hardening [11,26]. This may account for the hardness reduction of the aged alloy pre-precipitated at a lower temperature. Compared with NP alloy, the tensile strengths of 440P and 420P alloys decrease by ~5% (Table 2). This can be explained from the size of precipitates within the grains. Seen from Fig. 6, at NP alloy temper, the precipitates with a size of 5−8 μm within the grains are distributed homogeneously. Compared to NP temper, however, the size of precipitates within the grains increases slightly (size of 8−12 μm).

5 Conclusions

1) HTPP treatment substantially enhances the distribution discontinuity of the coarse GBPs, which cannot act as an active intergranular corrosion channel accounting for the improved SCC and IGC resistance, and the coarsening and interspacing effect on GBPs becomes more obvious with decreasing the pre-precipitation temperature.

2) The $I_{SCC}(\delta)$ decreases from 25.75% to 8.41% at the expense of ~5% tensile strength after pre-precipitation treatment, while the tensile strength of 420P alloy is basically the same as that of 440P alloy; the susceptibility to IGC reduces by decreasing the maximum attack depth from 53.6 to 19.8 μm.

3) The φ_{corr} of the pre-precipitation ones is slightly negative compared to NP alloy, but the J_{corr} is much lower than that of NP alloy. Further, the R_p is much greater than that of NP alloy. Among various alloy tempers, 420P alloy is the least sensitive to galvanic corrosion.

References

[1] EINZ A, HASZLER A, KEIDEL C, MOLDENHAUER S, BENEDICTUS R, MILLER W S. Recent development in aluminum alloys for aerospace applications [J]. Materials Science and Engineering A, 2000, 280(1): 102−107.

[2] LI Jin-feng, PENG Zhuo-wei, LI Chao-xing, JIA Zhi-qiang, CHEN Wen-jing, ZHENG Zi-qiao. Mechanical properties, corrosion behaviors and microstructures of 7075 aluminum alloy with various aging treatments [J]. Transactions of Nonferrous Metals Society of China, 2008, 18(4): 755−762.

[3] KANNAN M B, RAJA V S, RAMAN R, MUKHOPADHYAY A K. Influence of multi-step aging on the stress corrosion cracking behavior of 7010 Al alloy [J]. Corrosion, 2003, 59: 881−889.

[4] CHEN Song-yi, CHEN Kang-hua, DONG Peng-xuan, YE Sheng-ping, HUANG Lan-ping. Effect of heat treatment on stress corrosion cracking, fracture toughness and strength of 7085 aluminum alloy [J]. Transactions of Nonferrous Metals Society of China, 2014, 24(7): 2320−2325.

[5] PENG Guo-sheng, CHEN Kang-hua, CHEN Song-yi, FANG Hua-chan. Influence of dual retrogression and re-aging temper on microstructure, strength and exfoliation corrosion behavior of Al−Zn−Mg−Cu alloy [J]. Transactions of Nonferrous Metals Society of China, 2012, 22(4): 803−809.

[6] NAJJAR D, MAGNIN T, WARNER T. Influence of critical surface defects and localized competition between anodic dissolution and hydrogen effects during stress corrosion cracking of a 7050 aluminum alloy [J]. Materials Science and Engineering A, 1997, 238(2): 293−302.

[7] SCAMANS G M, HOLROYD N J H, TUCK C D S. The role of magnesium segregation in the intergranular stress-corrosion cracking of aluminum-alloys [J]. Corrosion Science, 1987, 27(4): 329−347.

[8] KNIGHT S P, BIRBILIS N, MUDDLE B C, TRUEMAN A R, LYNCH S P. Correlations between intergranular stress corrosion cracking, grain-boundary microchemistry, and grain-boundary electrochemistry for Al−Zn−Mg−Cu alloys [J]. Corrosion Science, 2010, 52(12): 4073−4080.

[9] LIN J C, LIAO H L, JEHNG W D, CHANG C H, LEE S L. Effect of heat treatment on the tensile strength and SCC-resistance of AA7050 in an alkaline saline solution [J]. Corrosion Science, 2006, 48(10): 3139−3156.

[10] OU B L, YANG J G, WEI M Y. Effect of homogenization and aging treatment on mechanical properties and stress-corrosion cracking of 7050 alloys [J]. Metallurgical and Materials Transactions A, 2007, 38(8): 1760−1773.

[11] CHEN Song-yi, CHEN Kang-hua, PENG Guo-sheng, LIANG Xin, CHEN Xue-hai. Effect of quenching rate on microstructure and stress corrosion cracking of 7085 aluminum alloy [J]. Transactions of Nonferrous Metals Society of China, 2012, 22(1): 47−52.

[12] HUANG Lan-ping, CHEN Kang-hua, LI Song. Influence of grain-boundary pre-precipitation and corrosion characteristics of inter-granular phases on corrosion behaviors of an Al−Zn−Mg−Cu alloy [J]. Materials Science and Engineering B, 2012, 177(11): 862−868.

[13] HUANG Lan-ping, CHEN Kang-hua, LI Song, LIU Hong-wei. Effect of high-temperature pre-precipitation on microstructure, mechanical property and stress corrosion cracking of Al−Zn−Mg aluminum alloy [J]. The Chinese Journal of Nonferrous Metals, 2005, 15(3): 727−733. (in Chinese)

[14] SHI Yun-jia, PAN Qing-lin, LI Meng-jia, HUANG Xing, LI Bo. Influence of alloyed Sc and Zr, and heat treatment on microstructures and stress corrosion cracking of Al−Zn−Mg−Cu alloys [J]. Materials Science and Engineering A, 2015, 621: 173−181.

[15] RAMGOPAL T, GOUMA P I, FRANKLE G S. Role of grain boundary precipitates and solute-depleted zone on the intergranular corrosion of aluminum alloy 7150 [J]. Corrosion, 2002, 58: 687−697.

[16] LIU Sheng-dan, CHEN Bin, LI Cheng-bo, DAI Yun, DENG Yun-lai, ZHANG Xin-ming. Mechanism of low exfoliation corrosion resistance due to slow quenching in high strength aluminum alloy [J]. Corrosion Science, 2015, 91: 203−212.

[17] GB/T 7998−2005. Test method for intergranular corrosion of aluminum alloy [S]. (in Chinese)

[18] DU X S, SU Y J, LI J X, QIAO L J, CHU W Y. Stress corrosion cracking of A537 steel in simulated marine environments [J]. Corrosion Science, 2012, 65: 278−287.

[19] GABRIELE R. Corrosion rate monitoring by linear polarization method [J]. Corrosion Science, 1993, 34: 2031−2044.

[20] TANG Jian-guo, CHEN Hui, ZHANG Xin-ming, LIU Sheng-dan, LIU Wen-jun, OUYANG Hui, LI Hong-ping. Influence of quench-induced precipitation on aging behavior of Al−Zn−Mg−Cu alloy [J]. Transactions of Nonferrous Metals Society of China, 2012, 22(6): 1255−1263.

[21] KOMISAROV V, TALIANKER M, CINA B. The effect of retrogression and reaging on the resistance to stress corrosion of an 8090 type aluminum alloy [J]. Materials Science and Engineering A, 1996, 221(1−2): 113−121.

[22] TALIANKER M, CINA B. Retrogression and reaging and the role of dislocations in the stress corrosion of 7000-type aluminum alloys [J]. Metallurgical and Materials Transactions A, 1989, 20(10): 2087−2093.

[23] MOREIRA A H, BENEDETTI A V, SUMODJO P T A, GARRIDO J A, CABOT P L. Electrochemical behavior of heat-treated Al−Zn−Mg alloys in chloride solutions containing sulphate [J]. Electrochimica Acta, 2002, 47: 2823−2831.

[24] DENG Y, YIN Z M, ZHAO K, DUAN J Q, HU J, HE Z B. Effects of Sc and Zr microalloying additions and aging time at 120 °C on the corrosion behavior of an Al−Zn−Mg alloy [J]. Corrosion Science, 2012, 65: 288−298.

[25] WANG Zhu-tang, TIAN Rong-zhang. Handbook of aluminum alloy and its working [M]. 3rd ed. Changsha: Central South University Press, 2000. (in Chinese)

[26] DUMONT D, DESCHAMPS A, BRECHET Y. On the relationship between microstructure, strength and toughness in AA7050 aluminum alloy [J]. Materials Science and Engineering A, 2003, 356(1−2): 326−336.

晶界预析出处理对 Al−Zn−Mg 合金抗腐蚀性能的影响

李慧中 [1,2,3]，姚三成 [1]，梁霄鹏 [1,2,3]，陈永辉 [1]，刘 超 [1]，黄 岚 [3]

1. 中南大学 材料科学与工程学院，长沙 410083；
2. 中南大学 有色金属材料科学与工程教育部重点实验室，长沙 410083；
3. 中南大学 粉末冶金国家重点实验室，长沙 410083

摘 要：通过常温拉伸、晶间腐蚀、慢应变速率应力腐蚀等试验，并结合电子显微观察，研究常规固溶后在不同温度下高温预析出处理对 7005 铝合金力学性能、腐蚀行为及显微组织的影响。结果表明：合金的维氏硬度随着预析出温度的降低而逐渐下降，而电导率则呈现出相反的变化趋势，并以此选择 440 和 420 °C 进行预析出对比研究。高温预析出能显著增加晶界粗大析出相的不连续分布程度，且随着预析出温度的降低，晶界析出相的粗化和不连续程度增加，致使合金抗晶间腐蚀和应力腐蚀性能得到显著提高，而强度略有下降。

关键词：7005 铝合金；晶界预析出；应力腐蚀开裂；晶间腐蚀；显微组织

(Edited by Yun-bin HE)